

FEDSM99-7178

BUOYANCY INDUCED FLOW IN A VERTICAL COMBUSTION DISCHARGE DUCT

Mihai G. BURZO, Dani FADDA, and Peter E. RAAD
 Mechanical Engineering Department, Southern Methodist University
 Dallas, Texas 75275-0337, USA
 Tel: +214-768-3043; Fax: +214-768-1473; Email: peter@seas.smu.edu

Keywords: *Buoyancy-induced flow, natural convection, numerical simulation, instability.*

ABSTRACT

Hot exhaust gas flows upwardly in a vertical duct and discharges at the top of the duct into the cold atmosphere. The rising hot gas is subject to cooling at the duct sidewalls and open top. Buoyancy-induced secondary flow patterns are observed and analyzed in this work. Results of this numerical investigation indicate the existence of four distinct flow regimes, three of which are steady while the last is quasi-steady. Since the flow is characterized by the Reynolds and Rayleigh numbers, a map of the observed flow regimes is presented in terms of these two variables.

INTRODUCTION

Fluid flow in the vertical exhaust gas duct, presented in Fig. 1, is investigated in this work. The hot gas inlet at the bottom of the domain, shown in Fig. 1, receives hot gas from below.

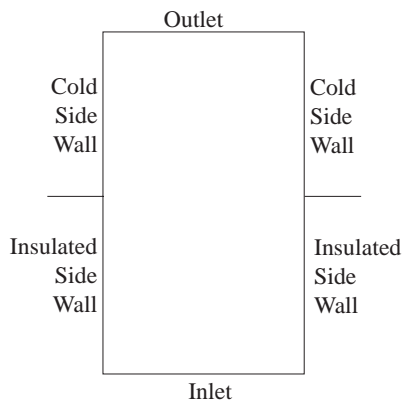


Fig. 1 Chimney

The outlet is at the top and discharges to the cold atmosphere. The sidewalls are protected from the cold outdoor temperatures under a horizontal roof (shown as a thin horizontal line in Fig. 1) while being exposed to the cold atmosphere above the roof. The duct identified in Fig. 1 exhibits vertical symmetry. The rectangular cavity presented in Fig. 2 represents a symmetrical half of the duct. Symmetry boundary conditions are fixed at the right boundary while isothermal and adiabatic conditions are prescribed at the higher and lower portions of the left boundary wall, respectively. A parabolic profile is set for the inlet velocity at the bottom boundary forcing the hot gas to flow upwardly. The outlet is prescribed at the top where the hot gas is discharged to the cold atmosphere.

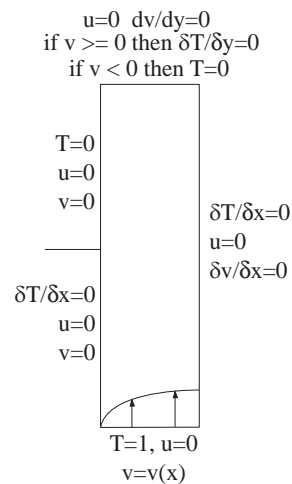


Fig. 2 Cavity

The flow is characterized by the Reynolds (Re), Prandtl (Pr), and Rayleigh (Ra) numbers. The fluid considered in this

investigation is one with a constant Prandtl number equal to 0.7. The Reynolds and Rayleigh numbers, however, are varied ($Ra \in [5.83 \times 10^4, 1.75 \times 10^6]$ and $Re \in [0, 1000]$) and their effects on the flow patterns are investigated.

Buoyancy-induced convection heat transfer has been the subject of many studies published by several authors. Patterson and Imberger (1980), and Lage and Bejan (1991) discussed fluid flow in a rectangular enclosure subject to differentially heated isothermal sidewalls and constant gravitational acceleration. These authors studied the effects of the fluid properties on the transient heat transfer in the enclosure. De Vahl Davis and Jones (1982) focused on the steady-state flow for the same type enclosure and published a collection of invited contributions by many researchers who used different numerical methods to solve a benchmark set of problems. Cheng et al. (1995) studied the buoyancy-induced flow reversal phenomenon in the developing region of a vertical rectangular duct. They found that the strength and the extent of the reverse flow are dependent mainly on the ratio of the Grashof and Reynolds numbers (Gr/Re), and the aspect ratio of the cross section. Due to the buoyancy-assisted flow effects, an adverse pressure gradient develops downstream as Gr/Re becomes sufficiently high. Janssen et al. (1993) studied the three dimensional effects on periodic oscillations in a cubical cavity, using the finite-volume method. Janssen concluded that the calculated frequency was almost the same as for the 2D square cavity. However, a strong three-dimensionality in the distribution of the amplitude has been observed. Vafai and Etefagh (1990) studied thermal and fluid flow instabilities in buoyancy-driven flow in open-ended cavities. They showed that at high Rayleigh number, a one-to-one relationship exists between the frequency of the periodic oscillations in the Nusselt number, on one hand, and the oscillations and position inside the cavity of the central vortex, on the other hand. In fact, they conclude that the frequency of oscillations of the Nusselt number increases linearly as the Rayleigh number increases.

The current work is a thorough investigation of the effects of *both* the Re and Ra numbers on the upward flow. Specifically, four distinct flow regimes are observed and identified. A complete description of the observed flow patterns is presented below after a brief discussion of the numerical method used.

NOMENCLATURE

C	specific heat
d	duct width
g_y	gravitational acceleration
k	thermal conductivity
p	pressure
T	temperature
T_o	reference temperature
U	average inlet vertical up flow velocity
u, v	velocity components

Non-Dimensional

Re	Reynolds number = $\rho U d / \mu$,
Pr	Prandtl number = $\nu / \alpha = 0.7$
Ra	Rayleigh number = $\rho \beta d^3 \Delta T g_y / (\mu \alpha)$

Greek

α	thermal diffusivity = $k / (\rho C)$
β	thermal expansion coefficient
ΔT	temperature difference between hot gas and cold atmosphere
μ	dynamic viscosity
ν	kinematic viscosity
ρ	density

NUMERICAL METHOD

A new computer simulation program is written based on the SMMC-E method (Raad and Fadda, 1997) for free surface flow simulations. The fluid momentum is computed by a direct solution of the full Navier-Stokes equations, coupled with the continuity equation. In two spatial dimensions, these equations appear as:

$$\rho \left(\frac{\partial u}{\partial t} + u \frac{\partial u}{\partial x} + v \frac{\partial u}{\partial y} \right) = -\frac{\partial p}{\partial x} + \mu \left(\frac{\partial^2 u}{\partial x^2} + \frac{\partial^2 u}{\partial y^2} \right) - \rho g_x \quad (1)$$

$$\rho \left(\frac{\partial v}{\partial t} + u \frac{\partial v}{\partial x} + v \frac{\partial v}{\partial y} \right) = -\frac{\partial p}{\partial y} + \mu \left(\frac{\partial^2 v}{\partial x^2} + \frac{\partial^2 v}{\partial y^2} \right) - \rho g_y \quad (2)$$

$$\frac{\partial u}{\partial x} + \frac{\partial v}{\partial y} = 0 \quad (3)$$

The heat transfer is computed by a solution of the energy equation shown below coupled with the above momentum and continuity equations:

$$\frac{\partial T}{\partial t} + u \frac{\partial T}{\partial x} + v \frac{\partial T}{\partial y} = \alpha \left(\frac{\partial^2 T}{\partial x^2} + \frac{\partial^2 T}{\partial y^2} \right) \quad (4)$$

The transient momentum equations represent a balance of inertia, pressure, viscous, and gravitational forces. The Oberbek-Boussinesq approximation is introduced to link the momentum and energy equations. With this approximation, the fluid density appearing in the inertia terms is held constant while the density that appears in the gravitational terms is considered to vary with the temperature according to the following relation:

$$\rho = \rho_0 [1 + \beta (T - T_0)] \quad (5)$$

A projection method is used to solve the momentum equations along with the mass conservation equation on a rectangular, Eulerian grid. The first step in this method is a computation of tentative velocities from the momentum equations in the absence of all pressure terms. While the absence of the pressure terms does not affect the vorticity of the flow, the continuity equation is normally not satisfied. The buoyancy terms in this first step are computed by using the current (or most recent) temperature field. An incompressibility deviation function is calculated from the tentative velocity field, yielding local measures of the non-satisfaction of the continuity principle for each control volume in the Eulerian mesh. The computed incompressibility deviation function is then used as the non-homogeneous source term in a pressure Poisson equation to calculate a pressure correction field. Finally, the tentative velocities are corrected by the use of the gradients of this pressure field, resulting in velocities that satisfy both the momentum and continuity equations without altering the vorticity field.

After advancing the velocity field a small interval in time, the energy equation is solved by the control volume method described by Patankar (1980) in order to update the temperature field. The computational cycle is repeated and the solution is marched in time for a prescribed desired duration.

SOLUTION ACCURACY

Numerical results generated from this simulation program are benchmarked against several natural convection problems available in the literature. Specifically, a variety of cavity problems with isothermal vertical walls and insulated horizontal walls were considered. Comparisons between simulation results and published data (Lage and Bejan (1991), Davis and Jones (1982), and Patterson and Imberger (1980)) demonstrate both-steady state and transient accuracy.

Grid and temporal accuracy for the problem discussed herein were also tested. A uniform, staggered, grid of rectangular cells was used, the size of which was varied between 10×40, 20×80, and 30×120. Effects of the grid size on the flow field were observed and indicated that the 20×80 grid is sufficient to accurately resolve the flow considered. The time step used in marching the solution was computed such that the product of maximum velocity by the time step is less than a

third of the grid spacing, or in other words, the Courant number is less than 1/3. The 20×80 grid is used in all numerical simulations presented in this paper.

RESULTS

A large number of cases was considered in this investigation, eighteen (18) of which are presented here for Rayleigh number values of $Ra = 5.83 \times 10^4$, 5.83×10^5 , and 1.75×10^6 . For each value of the Rayleigh number, six (6) values of the Reynolds number are presented; namely $Re = 0, 12.5, 25, 175, 250,$ and 750 .

A map of the observed thermal boundary layers is presented in Fig. 3 as a function of the non-dimensional governing variables, Re and Ra . This map offers a visual summary of all the cases considered in this work. In each isotherm plot, the cold (0) and hot (1) regions are identified. The bottom row corresponds to $Ra = 5.83 \times 10^4$. As Re is decreased, a transition from regime 1 to regime 2 is observed. The middle row corresponds to $Ra = 5.83 \times 10^5$. As Re is decreased, the transition from regime 1 to regime 2 and then to regime 3 is observed. Finally, the top row corresponds to $Ra = 1.75 \times 10^6$. Regime 1, at this level of Ra , is expected to occur at high Re values beyond the range considered in this work. The transitions from regime 2 to regime 3 and then to regime 4 are observed as Re is decreased.

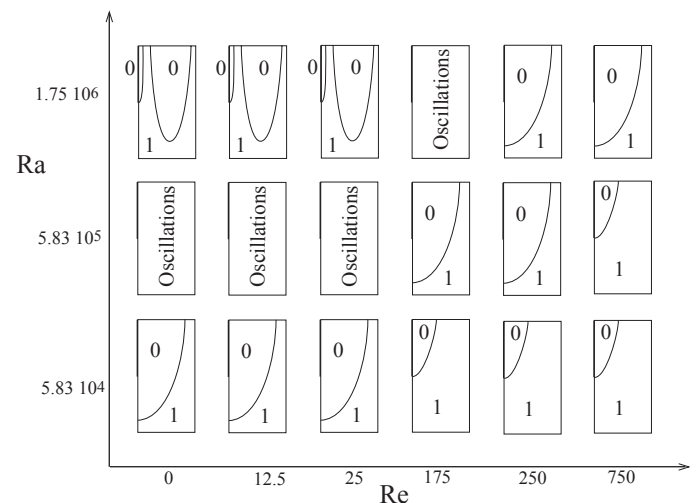


Fig. 3 Schematics of the Thermal Boundary Layers Characterizing Four Flow Regimes

Briefly, Regime 1 corresponds to a thin thermal boundary layer developed near the cold wall, typical of forced convection, while Regime 2 is characterized by a drop of the thermal boundary layer caused by the outlet cold temperature. Regime 3 is one of quasi-steady oscillations. The top outlet cold temperature is the driving mechanism in Regime 4, while the cold side has a minor effect on the pattern of the flow.

Numerical results characterizing the different flow regimes are presented below in detail.

Low Rayleigh Number: $Ra = 5.83 \times 10^4$. For a Rayleigh number of 5.83×10^4 two distinct flow regimes are observed over the entire range of Reynolds number considered ($Re \in [0, 750]$). The two regimes are represented in Fig. 4 as contour plots of the isotherms and streamlines with (a) high and (b) low Reynolds numbers.

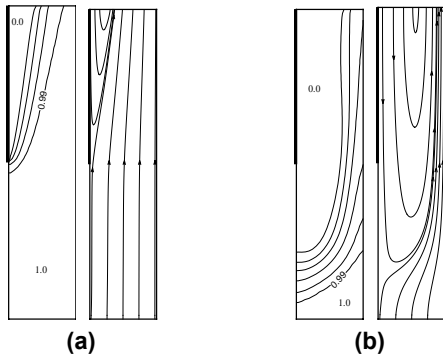


Fig. 4 Isotherms (left) and streamlines (right) $Ra=5 \times 10^4$, (a) $Re=250$ and (b) $Re=25$

Closely observing the isotherm (left) and stream function (right) contour plots in Fig. 4(a) points to the existence of a thermal boundary layer near the cold wall. This boundary layer is typical of forced convection heat transfer near a wall and its thickness may be easily predicted both numerically and analytically. Observing the streamlines indicates that the buoyancy forces corresponding to this layer only slightly affect the up-ward flow in the immediate vicinity of the cold wall. This first flow regime is referred to as Regime 1. Observing the contours presented in Fig. 4(b), however, one notes that the thermal boundary layer drops downwards causing significant buoyancy-induced flow recirculation in the cavity. This second flow regime is referred to as Regime 2.

Intermediate Rayleigh Number: $Ra = 5.83 \times 10^5$. Results corresponding to $Ra = 5.83 \times 10^5$ indicate the existence of three different flow regimes. Specifically, the regimes correspond to high up-flow velocity ($Re \geq 750$), medium up-flow velocity, and low up-flow velocity ($Re \leq 25$). Contour plots of the streamlines and isotherms corresponding to the first two regimes ($Re = 750$ and 175) are presented in Fig. 5. The plots presented in Fig. 5 are similar to those presented in Fig. 4, above, indicating similar fluid flow behavior at the two Ra numbers ($Ra = 5.83 \times 10^4$ and 5.83×10^5). The third regime (Regime 3) occurs at lower Re and is one of quasi-steady oscillation. For the case of $Ra=5.8 \times 10^5$ and $Re=12.5$, the period of oscillation is equal to 4.38 minutes.

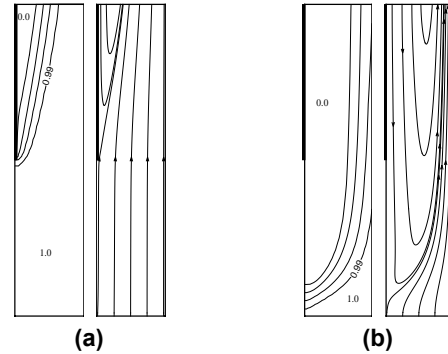


Fig. 5 Isotherms (left) and streamlines for (right) $Ra=5 \times 10^5$, (a) $Re=750$ and (b) $Re=175$

A complete set of isotherms is presented in Fig. 6 representing the temperature contours during one period of oscillation.

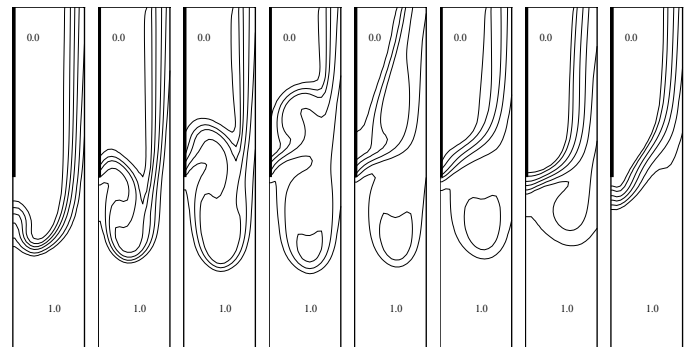
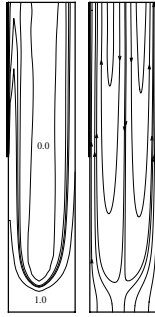


Fig. 6 Isotherms During One Period of Oscillation ($Ra=5.8 \times 10^5$ and $Re=12.5$)

Further computations in this low Reynolds number regime ($Re \leq 25$) indicate that the period of oscillation is not dependent on the actual value of the Reynolds number. The oscillations persist as Re is lowered to $Re = 0$ (bottom of the duct is closed). The source and reason of the observed oscillations are easily understood at the higher level of Rayleigh number as shown next.

High Rayleigh Number: $Ra = 1.75 \times 10^6$. Results corresponding to $Ra = 1.75 \times 10^6$ indicate the existence of all three regimes observed above, in addition to a different (fourth) flow regime. This fourth regime is observed at the low end of the considered range of Reynolds numbers. Isotherms and contour plots characterizing the flow in this fourth regime are presented in Fig. 7.



**Fig. 7 Isotherms (left) and streamlines (right)
Ra=1.75×10⁶, (a) Re=25**

Close observations of the contour plots presented in Fig 7 indicate that the top outlet cold temperature is the driving mechanism causing buoyancy induced flow while the cold sidewall has a relatively minor effect.

The temperature at the top centerline of the duct (top right corner of the symmetrical computational domain) is recorded for all the considered cases and its value is plotted in Fig. 8. At high values of Reynolds number ($Re \geq 750$) a single curve with a value of 1.0 indicates that cooling does not affect the fluid temperature at the duct centerline. For $Ra = 5.83 \times 10^4$, steady-state flow is indicated by single temperature values in Fig. 8 for the entire range of Re . Moreover, this temperature remains equal to 1.0 as Re is decreased and then decreases abruptly as the thermal boundary layer thickness reaches half the duct width.

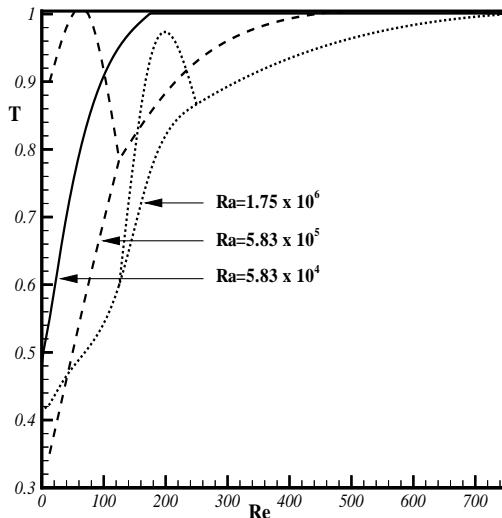


Fig. 8 Duct Top Centerline Temperature (top right corner of the symmetrical computational domain)

The results of Fig. 8 that correspond to $Ra = 1.75 \times 10^6$ and 5.83×10^5 indicate a decrease in the temperature as Re is decreased. A split is observed in these two curves as Re is decreased further indicating flow oscillations (Regime 3) between maximum and minimum temperature values plotted in Fig. 8.

An explanation of the computed flow oscillations previously referred to as regime 3 is obtained by closely examining the isotherms at the top row of Fig. 3 ($Ra = 1.75 \times 10^6$). Specifically, these oscillations are a result of secondary buoyancy-induced flow overpowering the forced upward flow. At high Re , the upward flow reduces the effects of the outlet cooling while the natural convection due to the cold sidewall steadily dominates. At low Re , however, the volume of upflowing fluid is minor, allowing appreciable steady-state natural convection due to the cold outlet. Between the two regimes, the outlet and sidewall effects are comparable, making steady-state flow impossible to sustain. Finally, as Re approaches zero, a single line is observed (Fig. 8) corresponding to $Ra = 1.75 \times 10^6$ indicating the steady-state flow behavior referred to as Regime 4.

CONCLUSION

The upflow of a hot gas in a vertical duct is considered. The sidewalls of the duct extending above a horizontal ceiling are cold as the duct outlet discharges fluid into the cold atmosphere. Four different flow regimes are observed and their existence is mapped as a function of the values of Re and Ra . Regime 1 corresponds to high values of Re and is characterized by a thin thermal boundary layer near the cold walls. As Re is decreased, or Ra is increased, the thermal boundary layer thickness increases. Regime 2 is observed when the thermal boundary layer becomes heavy and results in buoyancy-induced downward flow near the wall. As Re is decreased and Ra is increased, a new regime is observed. Regime 4 corresponds to buoyancy-induced downward flow from the top outlet. An oscillatory regime, Regime 3, is a transition regime of distinct behavior observed between regimes 2 and 4.

ACKNOWLEDGMENTS

The authors acknowledge the support of the Mechanical Engineering Department at Southern Methodist University, which made this project possible.

REFERENCES

- Cheng, C. H., Weng, C. J., and Aung, W., 1995, "Buoyancy Effects on the Flow Reversal of Three Dimensional Developing Flow in a Vertical Rectangular Duct – A Parabolic Model Solution," Transactions of ASME, Vol. 117, pp. 238-241.
- Davis, G. de Vahl and Jones, I. P., 1983, "Natural convection in a square cavity: a comparison exercise", International Journal Numer. Meth. Fluids, Vol. 3, pp. 227-248.

Janssen, R.J.A., Henkes, R. A. W. M., and Hoogendoorn, C. J., 1993, "Transition to Time Periodicity of a Natural-Convection Flow in a 3D Differentially Heated Cavity," *International Journal of Heat and Mass Transfer*, Vol. 36, No. 11, pp. 2927-2940.

Lage, J. L. and Bejan, A., 1991, "The Ra-Pr Domain of Laminar Natural Convection in an Enclosure Heated From the Side," *Numerical Heat Transfer*, Vol. 19, Part A, pp. 21-41.

Patankar, S. V., 1980, *Numerical Heat Transfer and Fluid Flow*, Hemisphere Publishing Corp., New York.

Patterson, J., and Imberger, J., 1980, "Unsteady Natural Convection in a Rectangular Cavity," *Journal of Fluid Mechanics*, Vol. 100, Part 1, pp. 65-86.

Raad, P. E. and Fadda, D., 1997, "Free Surface Mixing with Heat Transfer", *Numerical Heat Transfer: Applications*, Vol. 31, pp. 685-702.

Vafai, K. and Etefagh, J., 1990, "Thermal and Fluid Flow Instabilities in Buoyancy-Driven Flows in Open Ended Cavities," *International Journal of Heat and Mass Transfer*, Vol. 33, No. 10, pp. 2329-2344.